MEMS-Based Satellite Micropropulsion Via Catalyzed Hydrogen Peroxide Decomposition

Darren L. Hitt[1] Charles M. Zakrzwski[2] Michael A. Thomas[2,*]

August 30, 2001

[1]Department of Mechanical Engineering

The University of Vermont

Burlington VT 05405

(Corresponding Author)

[2]Propulsion Branch

Guidance, Navigation & Control Center

NASA Goddard Space Flight Center

Greenbelt MD

*Presently: 1st Lt., United States Air Force

Columbus Air Force Base

Columbus, MS 39705

ABSTRACT

Micro-electromechanical systems (MEMS) techniques offer great potential in satisfying the mission requirements for the next generation of "micro-scale" satellites being designed by NASA and Department of Defense agencies. More commonly referred to as "nanosats", these miniature satellites feature masses in the range of 10-100 kg and therefore have unique propulsion requirements. The propulsion systems must be capable of providing extremely low levels of thrust and impulse while also satisfying stringent demands on size, mass, power consumption and cost. We begin with an overview of micropropulsion requirements and some current MEMS-based strategies being developed to meet these needs. The remainder of the article focuses the progress being made at NASA Goddard Space Flight Center towards the development of a prototype monopropellant MEMS thruster which uses the catalyzed chemical decomposition of high concentration hydrogen peroxide as a propulsion mechanism. The products of decomposition are delivered to a micro-scale converging/diverging supersonic nozzle which produces the thrust vector; the targeted thrust level approximately 500 N with a specific impulse of 140-180 seconds. Macro-scale hydrogen peroxide thrusters have been used for satellite propulsion for decades; however, the implementation of traditional thruster designs on a MEMS scale has uncovered new challenges in fabrication, materials compatibility, and combustion and hydrodynamic modeling. A summary of the achievements of the project to date is given, as is a discussion of remaining challenges and future prospects.

1 Introduction

1.1 The Need for Satellite Micropropulsion

Owing to current trends in NASA and military space missions, there is an increasing demand for the ability to provide extremely low levels of thrust or "micropropulsion". The need for micropropulsion arises in essentially two distinct, yet related settings. In the first scenario, a more traditional-scale type of satellite is required to maintain its orbital attitude and position to an extremely high degree of precision for purposes of alignment. Extremely small perturbations to the attitude and/or position of the satellite may result because of such effects as solar radiation pressure or gravitational nonuniformities. To offset the perturbations, periodic (or continuous) thrust corrections on the order of micro-Newtons may be required. It is important to note that the primary propulsion challenge here is to develop a thruster capable of delivering the low thrust level; there are no severe constraints on size, mass, or power requirements and the satellite itself can be sizeable.

The second scenario in which micro-scale levels of thrust is required is when the *size of the satellite is itself significantly reduced.* It is this setting that will be the focus of this article. There is an overall movement towards the development of "small-" (<100 kg) and "nano-" (<10 kg) sized spacecraft which can be used in a number of applications. One of the most promising applications is the use of distributed spacecraft formations to achieve specific mission goals. Distributed spacecraft concepts such as "formation flying" represents a departure from traditional satellite philosophy which was based on a single, massive multi-functional spacecraft. An excellent example of such a mission is NASA's Laser Interferometry Space Antenna (LISA) program which is intended to detect gravitational waves in the solar system; details on the LISA Program can be found at the NASA/Jet Propulsion Laboratory website.[1] In the LISA mission, three satellites having individual masses of 500 kg are stationed at a stable Lagrange point (L5) in the solar system (where the gravitational force from the

[1] lisa.jpl.nasa.gov

Earth and Sun are equal) in a triangular formation separated by 5,000,00 km and must maintain mutual alignments of 30 nrad and orbital positions within 10 nm. With this level of precision, the perturbation of the radiation pressure from the solar wind is sufficient to upset the operation and must be offset by a thrust levels ranging between 1-100 N with an estimated accuracy of 0.1 N. In the LISA mission, it is planned that only about 50 grams of propellant will be required for its miniaturized field-emission electric (FEEP) engines during its five year mission.

Distributed spacecraft mission architectures offer a number of advantages such as reduced mission cost (production and launch), increased flexibility and reliability, and improved data resolution (e.g., Moser et al., 1999; Weidow and Bristow, 1999) . Owing to the substantially reduced size, the nano-sized satellites ("nanosats") have unique propulsion requirements, including extremely low thrust levels and/or extremely low minimum impulse requirements for orbital maneuvers and attitude control (Blandino and Cassady, 1998; Pollard et al., 1999). Propulsion systems for these satellites, aside from the thrust and impulse requirements, must also satisfy additional mass, volume and power constraints. A listing of typical operating parameters is given in Table 1.

Because existing propulsion technology cannot meet many of the design constraints for nanosats (Mueller, 1997), the need to develop novel and miniaturized micropropulsion strategies has arisen. MEMS-based propulsion systems have been identified as potential solutions (Ketsdever and Mueller, 1998). MEMS-based thruster concepts are attractive because they offer the capability of effectively miniaturizing traditional thruster designs for nanosat application. This permits, in principle, micro-scale design parameters to be satisfied while drawing upon the wealth of technical expertise known about traditional satellite thruster design (although additional micro-scale physics may need to be incorporated). The potential advantages of developing a MEMS propulsion system are numerous. They can be extremely small, with dimensions on the micron scale; with the continuous evolution of microfabrication and nanofabrication techniques nano-scale thrusters may become a reality. The latter

is significant for the planned "pico-sats" (< 1 kg) of the future. Their construction can be made extremely lightweight with simple components and low dead volume. MEMS thrusters, like semiconductors, can be reproduced in mass quantities with a low cost per device. And, finally, a MEMS approach also allows for new and innovative approaches that take specific advantage of unique micro-scale geometries and/or physics - options that were not available or feasible for macro-scale thruster designs.

1.2 Brief Overview of Some Current Micropropulsion Concepts

Over the past few years numerous and diverse micropropulsion initiatives have been undertaken by the government, industry and academia. The various approaches, all of which tend to have their unique benefits, include chemical propellants, both liquid and solid and electric propulsion concepts, with the focus on electro-thermal concepts. A recent review of micropropulsion systems for formation flying applications can be found in Reichbach et al. (2001). As a specific example, one of the more notable advances thus far is the DARPA solid propellant "digital microthruster" (Lewis et al., 2000). This MEMS-based thruster features lead-styphnate as the solid propellant which is contained in miniaturized cavities etched in silicon. The propellant is ignited by passing a current through miniaturized, embedded resistive elements. The ignited solid propellant sublimates and expands outward through a nozzle. Other significant concepts being pursued include: cold gas systems at MIT (Bayt et al., 1997; Janson and Henry, 1999), the Aerospace Corporation (Janson and Henry, 1999) , and ESA; arrays of solid and bipropellant "digital" single shot thrusters at NASA/Glenn Research Center (Reed, 1998), TRW (Antonsson and Janson, 1998), and Honeywell; pumped bi-propellant engines at MIT and NASA/Glenn Research Center (Reed, 1998); resisto-jets being developed at The Aerospace Corporation (Janson et al., 1999), USC and AFRL (Spanjers, 1998); and vaporizing liquid and subliming solid thrusters at NASA/Jet Propulsion Laboratory. A summary of some current

micropropulsion concepts being developed by different research groups is presented in Table 2. This listing is meant to provide the reader with a sense of scope and research activity in this area and is not intended as a comprehensive review . The interested reader can find a recent comprehensive survey of microthruster options in Mueller (2000) and shorter review of electric propulsion activities in the United States academia in Gallimore (2001).

In assessing the relative merit of a given approach, it is important to recognize that each mission specification will have its own set of unique constraints; one micropropulsion strategy might be an excellent fit for one type of mission but be inappropriate for another. Electrical-based microthrusters (e.g., pulsed-plasma thrusters/PPT, ion engines, field-emission electrical propulsion/FEEP) are capable of delivering extremely low thrust levels but currently are large in size and mass, and have relatively high power requirements with respect to nanosat concepts which have less than 10W total spacecraft bus power. At present, there are at least conceptual designs for scaling these types of devices to the MEMS level. Solid propellent devices (digital microthruster) are limited primarily by their digital nature: once fired they are not reusable. These devices therefore are constructed in arrays ("blister packs") and necessarily have a pre-set number of firings in their lifetime. Another potential problem in nanosat applications, the *location* of the thrust vector will vary from firing to firing as the devices are depleted. On a nanosat scale, the shift in the thrust location can produce additional perturbations to the attitude of the satellite which must be accounted for in each firing. Chemical propellants (e.g. hydrazine, hydrogen peroxide) have traditionally been attractive for satellites because they offer relatively high thrust-to-weight ratios owing to the inherently high amount of stored chemical energy per unit mass. This benefit is compounded in MEMS-scale devices because of the interplay of volume and surface area scaling. The mass of propellant is a volumetric quantity which decreases as the cube of the length scale; in contrast, thrust is a surface quantity which depends on the surface area of the nozzle outlet and so decreases as the square of the length scale. Thus the thrust-to-weight ratio

increases linearly with decreases in the device size. Another advantage of chemical thrusters is that they offer a greater range of total impulse, thrust level, and impulse bit than discrete solid propellant thrusters. We note that there are also certain considerations particular to the use chemical propellants, including chemical stability and safety, materials compatibility and shelf-life.

1.3 The NASA/GSFC Monopropellant Hydrogen Peroxide Microthruster

The possibility of a MEMS-based chemical monopropellant thruster has been identified in the propulsion literature (Janson, 1997; Mueller, 1997; Ketsdever and Mueller, 1999), and features certain advantages over liquid bi-propellant concepts. In terms of performance, monopropellant thrusters offer a greater range of total impulse, thrust level, and impulse bit; fabrication and propellant handling is also simpler than in bi-propellant systems. Despite the potential advantages, little work in this area has been reported. Monopropellant thrusters typically rely upon a catalyzed chemical decomposition of the liquid propellant as the source of energy. The chemical decomposition is a highly exothermic process which produces energetic gaseous reactants which expand and then exit through a micro-nozzle, providing a very small and precise impulse bit. The primary advantage of a liquid fueled system is that the thrust vectors are repeatable with an operational life proportional to the size of the external propellant tank. Further, the impulse bit from thruster can be controlled by regulating the propellant mass flow rate and/or duration; this results in a robust device capable of performing both attitude control and small orbital maneuvers.

At NASA/Goddard Space Flight Center (GSFC), work has focused on the development of a MEMS-based, catalytic monopropellant thruster concept which uses high-purity hydrogen peroxide (HTP for "high test peroxide") as the liquid propellant. The remainder of this article is devoted to describing the progress that has been made on this front, the challenges that remain, and the future

potential for this microthruster concept.

2 Design Considerations for a MEMS-based HTP Thruster

2.1 Operating Principle

The essential operating principle of the MEMS-based HTP thruster is straightforward and is illustrated in Figure 1. Liquid hydrogen peroxide of high purity (~90%) is fed from a propellant reservoir into through an injector which produces a desired pressure drop in the fluid. The injector feeds into the catalytic chamber where the liquid propellant undergoes a rapid chemical decomposition and produces high velocity gaseous products of reaction at the chamber outlet. The chemical decomposition is triggered by high-purity silver which serves as a surface catalyst. This type of mechanism has been used for decades in macro-scale satellite catalytic thrusters with other monopropellants, particularly hydrazine. The gas is then fed into a converging/diverging nozzle where the flow accelerates to a supersonic velocity ; the supersonic exit flow in turn produces the desired thrust vector. The overall design of a prototype MEMS/HTP thruster is an involved undertaking , drawing upon the disciplines of thermal, chemical-kinetic, and fluid-mechanical modeling, materials, and microfabrication techniques. In the sections to follow, important aspects from each of these areas are discussed which are essential in developing an operational design. To serve as a point of reference, mechanical drawings of two microthruster design configurations are shown in Figure 2a-b.

2.2 Chemical Decomposition of Hydrogen Peroxide

The mechanism for the propulsion is derived from the silver-catalyzed chemical decomposition of the hydrogen peroxide. The governing reaction for the decomposition process involving 100% hydrogen peroxide is:

$$2H_2O_2(\ell) \rightarrow 2H_2O\ (\ell) + O_2\ (g) + \text{heat}$$

The reaction features first-order chemical kinetics, with the rate of reaction being strongly dependent on temperature, HTP purity and concentration, and surface activity and less dependent on surface roughness and pH. The non-catalyzed reaction is quite slow and unsuitable for a thruster application, but pure silver provides an excellent catalyst which dramatically increases the reaction speed. The decomposition process is highly exothermic; for example, aqueous HTP at 85% concentration releases 586 calories of heat per gram at 25°C and the corresponding adiabatic flame temperature is approximately 613°C. The rate of decomposition also increases roughly 2.3× for each 10°C increase in temperature, and because the reaction is highly exothermic, the process accelerates. This latter statement assumes the heat removal is negligible, which is a valid assumption since the catalyzed reaction time scale is typically much smaller than time scale for external heat transfer.

2.3 Catalyst Chamber Design

The primary design task for the catalyst chamber is to identify an appropriate (optimal) size and configuration for the chamber which results in complete decomposition for a given mass flow rate of propellant. As the decomposition process is catalyzed by a surface reaction, a high surface area-to-volume ratio is warranted and which is well-suited for MEMS systems. In traditional, macro-scale thrusters this was achieved by passing the liquid propellant through catalyst-coated metallic screens or packed beds of pellets. Unfortunately, these options are not feasible in microchannels and new, alternative catalyst configurations are needed. Several catalyst geometries were considered in a fixed width, fixed length chamber configuration. The designs featured a wide, shallow channel with vertical walls or pillars which were coated with the silver catalyst and extended from the base to the top of the channel (see Figure 2). The approximate width of the channel designs was 1000 and the height ranged between 50-300 . For the purposes of microfabrication, only straight-sided channel walls and

pillars were considered. The objective was to create a maximum silvered surface area to enhance the rate of the decomposition; implicit in this undertaking is the assumption that the surface properties of the catalyst remain the same as in macro-scale thrusters. In this prototype, the upper surface is not coated because it will be used as a viewport for observing thruster operation; in future designs it too could be coated.

A key and challenging design question concerns the necessary length of the catalyst chamber to achieve complete decomposition of the HTP; this length must of course be capable with the overall MEMS specifications. The more intrinsic parameter is the *critical residence time* for the propellant to spend in the catalyst chamber; if known, this coupled with the mass flow rate determines the necessary length. Unfortunately, the critical residence time depends in a complicated way on the thermal and hydrodynamic conditions and is not well understood for the micro-scale geometry of a MEMS thruster. Lacking a sound theoretical basis on which to proceed, it was decided to use empirical catalyst lengths reported in the aerospace literature for macro-scale HTP thrusters and to scale those predictions to the MEMS scale (Bettner and Humble, 1998). The approach was to use these predictions to obtain order of magnitude estimates for the catalyst chamber length and then to proceed on an empirical basis. Using the empirical models, it was estimated that a length of 1.7-2mm would be required.

For the situation of incomplete decomposition combined with vaporization of the bulk fluid, an alternative prediction for the catalyst chamber length was proposed by Thomas et al. (2000). By considering a channel with only a silver-deposited bottom and regarding the surface decomposition of the HTP as a source of heat which generated a thermal boundary, an estimate of the catalyst chamber length could be roughly estimated as the downstream position at which the thermal boundary layer grew to equal the channel height. This scaling argument for a simplified geometry suggested a value of at least 1mm, and so was of the same order of magnitude as the empirical estimates.

To decouple pressure fluctuations in the catalyst chamber from the propellant feed system, an

injector was added to the thruster design to prevent back-flow (see Figure 2b). Located at the inlet to the catalyst chamber, the function is to reduce the propellant pressure through viscous losses. The injector essentially consists of a sequence of straight microchannels with 90-degree bends. The microchannels have a rectangular cross-section with a width of 29 and a depth of 50-300 depending on the particular design. The pressure drop consists of primary Poiseuille-type viscous losses which are particularly effective as this scales inversely with the fourth power of the microchannel hydraulic diameter; there are additional losses associated with the generation of secondary flows in the 90-degree bends. A pressure drop of approximately 20% is generally desirable for an injector, which amounts to ~1 psi for the present design (see Sect. 2.4). At the entrance to the injector is a row of "filter blocks" to trap any particulates that might be present in the propellant. While it is expected that the propellant will generally be free of such contaminants, the potential for even a small particulate to clog the nozzle (Section 2.4) warrants the inclusion of the filter. The filter blocks are vertical pillars with 50 square cross-sections with a gap spacing of 25 . Similarly, a manifold structure is included at the end of the injector. The manifold consists of a row of vertical pillars with rectangular cross-sections 65 by 40 with a gap spacing of 20 . The primary function of the manifold is to align and distribute the flow exiting the injector into the catalyst chamber.

2.4 Supersonic Nozzle

The thrust production for this device occurs in the converging/diverging supersonic nozzle (see Figure 2). The gaseous products of decomposition from the catalyst chamber are delivered to a converging nozzle where they accelerate to the local sonic velocity at the throat; the expansion part of the nozzle then accelerates the flow to supersonic speeds at the nozzle exit. For a steady-flow operation exhausting to space, the thrust produced is of the order

$$F \sim \dot{m} V_{\text{exit}}$$

where $\dot{m}$ is the mass flow rate and V_{exit} is the exit velocity. Another important parameter describing the thruster operation is the *specific impulse* I_{sp},

$$I_{sp} = \frac{F}{\dot{m}g}$$

which represents the thrust produced per unit weight of propellant consumed; this parameter though not dimensionless can also be regarded as a measure of the thruster efficiency.

A detailed discussion of the theoretical and computational aspects of the nozzle performance modeling is not the focus of the present article. Suffice to say that within the aerospace community there is a large knowledge base on the optimal design of traditional, macro-scale nozzles. In designing a MEMS-scale supersonic nozzle, however, there are certain considerations unique to the micro-scale that are important to note. First, owing to the nature of the microfabrication the nozzles are ducts with rectangular cross-sections and not axisymmetric like their macro-scale counterparts. Macro-scale thrusters often feature outlet nozzles with contoured walls (e.g., "bell" or "trumpet" shapes) for the purposes of straightening the outlet flow and producing a uniaxial thrust normal to the exit plane. Microfabrication of such contours is difficult and the current trend is to design the outlet to have straight walls with a specified divergence angle. Potential consequences of this is flow separation in the vicinity of the throat and expansion waves in the diverging section of the nozzle; the latter leads to thrust vector that may have significant lateral components resulting in a lower efficiency.

Secondly, flow in a MEMS supersonic nozzle can be substantially affected by viscous effects. This is evidenced by the Reynolds number of the flow, which is a measure of the relative magnitudes of inertial and viscous forces . To see this, the definition of the Reynolds number appropriate to these flows is

$$\mathrm{Re}^* = \frac{a^* D}{\nu^*},$$

where D is the throat width, and a* and * are the sonic velocity and kinematic viscosity, respectively, at the nozzle throat. For a HTP microthruster with a mass flow rate of 400 g/sec, one finds Re~450 at the throat. At this relatively low Reynolds, magnitude of viscous losses are significant and the viscous boundary layer extends away from the wall and into the bulk flow in the diverging nozzle section. The end result of the boundary layer growth is a choking of the mass flow rate and a reduction in thrust and efficiency. Detailed investigations of the role of viscous effects in MEMS thrusters have been performed by a number of authors both numerically (Zelesnik et al., 1994; Bayt et al., 1997; Bayt and Breuer; 1998;) and experimentally (Bayt et al., 1997; Choudhurri et al., 2001). A comprehensive review of these micronozzle flow behavior can be found in Bayt and Breuer (2001).

In the development of the thruster prototype, the target thrust level was 500 N. It was decided than approximate analysis of the thruster behavior would be sufficient and, to this end, a quasi-1D isentropic analysis of gas flow in the supersonic nozzle was performed. Assuming the products of the HTP decomposition are at the adiabatic flame temperature, the maximum specific impulse possible is determined by the relation (e.g. Saad, 1993)

$$I_{sp} = \sqrt{\frac{2\gamma R T_0}{g^2(\gamma - 1)}}$$

where is the ratio of the specific heats, R is the gas constant and T_0 is the stagnation temperature (i.e., the adiabatic flame temperature). The result is approximately 185 sec; we note here that empirical results from older studies suggest that a reduced value of ~140 sec is more likely to be observed based on an operating efficiency of 80% (Bureau of Aeronautics, 1955). Given the targeted thrust level and assuming the maximum possible specific impulse value, a mass flow rate of propellant equal to 275

g/sec is required. Because the products of decomposition are anticipated to inlet at a very low Mach number, a substantial area contraction is required to achieve the sonic conditions at the throat. A throat area of 9000- ^{2} was chosen for this design. For a thruster depth in the range of 100-300 , this corresponds to throat widths of 30-90 . While desirable to make the throat as small as possible, the geometric precision of the nozzle should not be compromised in the microfabrication. Assessing the microfabrication capabilities at NASA/GSFC, a conservative estimate was made that structures on the order of 20-30 were the smallest that would be admitted in the prototype design. We note in passing that this arguably over-conservative assessment was made in advance of the establishment of the microfabrication facility at NASA/GSFC. With the throat area fixed, an estimate of the required inlet pressure from the catalyst bed can be obtained according to (Hesse and Mumford, 1964)

$$P_{inlet} \sim \frac{\dot{m}}{A_t} \frac{\sqrt{\gamma R T_0}}{\gamma \left(\frac{2}{\gamma+1} \right)^{\frac{\gamma+1}{2\gamma-2}}}$$

with the result of approximately 5 psia. Finally, the divergence half-angle of expansion section of the nozzle was chosen in the range of 30 degrees based on viscous considerations. Results in the literature have suggested that low Reynolds micro-scale nozzles will perform better with larger divergence angles as opposed to the macro-scale designs typically featuring smaller divergence half-angles of 15-20 degrees (e.g., Bayt et al., 1997). The explanation is that at low Reynolds numbers the subsonic boundary layer in the nozzle exit will occupy a smaller percentage of the area for larger divergence angles. It is interesting to note that recent experimental work by Choudhurri et al. (2001) offers a somewhat competing view: they suggest that a smaller divergence angle should still be used for conical

nozzles because of the possibility of flow separation near the nozzle throat at larger divergence angles and moderate Reynolds numbers. Because it is not clear that flow separation will occur for the Reynolds number of the present design, the larger divergence angle was selected. A summary of the design and operating parameters of this nozzle are summarized in Table 3.

2.5 Microfabrication

The fabrication process consisted of three main steps: etching the thruster features, deposition of the silver catalyst, and bonding the cover glass to seal the assembly. Silicon wafers 10 cm in diameter and 500 m thick provided the substrate for the thruster; this size allows over 300 individual thrusters to be fabricated on a single wafer. Photographic mask designs were developed at NASA/GSFC which contained a variety of thruster designs. The photo-masks were then created (contractor) and patterned onto the silicon substrate using standard photolithographic methods. Etching of the substrate was performed using the deep reactive ion etching (DRIE) method and facilities at NASA Goddard Space Flight Center. The DRIE method was chosen for its capability of precisely etching vertical walls and structure deep into the substrate. Plumbing inlet ports for the propellant were created by back-etching a 1.0 mm hole in the silicon substrate. The next step was to then deposit high-purity silver (> 99.999%) on the surfaces forming the catalytic chamber. An aluminum shadow mask was used to cover the entire thruster except for the catalyst region. To ensure good adherence of the silver to the substrate, an intermediate 1 thick layer of titanium was vapor deposited on top of the the catalytic surfaces using an electron beam depositor operating in a vacuum chamber (1 torr). A layer of silver 1 thick was then similarly deposited on top of the titanium.

To seal the thruster, a glass (Pyrex) cover plate was anodically bonded to the silicon wafer. For thruster development purposes a glass plate was chosen to provide optical access to view the thruster operation during testing. The anodic bonding process was performed in a modified glove-box

arrangement. Argon gas was used to first purge the glove-box; any residual oxygen would oxidize the silver-coated surfaces of the wafer resulting in a much reduced surface activity of the catalyst. Once the purge was completed, the silicon-Pyrex stack was heated to 300-400° C and a negative voltage of 700-1200 V was applied to the Pyrex via a pinpoint contact while the silicon was kept grounded. The completed silicon-Pyrex wafer was then diced by diamond saw into the individual thrusters.

3 Results and Discussion

3.1 Microthruster Prototypes and Test Firings

A SEM photograph of the etched substrate for the thruster design with the diamond-pillar catalyst chamber is shown in Figure 3. At the top of this figure is the full thruster geometry, composed of an inlet reservoir, an injector, the catalyst chamber and the supersonic nozzle. Also shown in this figure are magnified images of the diamond-shaped vertical pillars in the catalyst chamber. In order to assess the quality and uniformity of the vertical RIE etching, some of the pillars have been intentionally destroyed to reveal features near the substrate bottom. At the bottom of this figure is a further magnification of the toppled pillars revealing the precision of the etching. A photograph of a finished and sealed single microthruster of the "diamond-pillar" design is shown in Figure 4; the device is approximately 0.5 cm square.

For the purposes of testing the fabricated thrusters, a slender stainless steel pipe (1.0 mm od) was fitted to back-etched hole in the silicon substrate to provide a plumbing connection. The pipe was then bonded to the thruster using a thermally conductive, electrically insulated polyimide epoxy. The first tests run on the completed thrusters were simple flow visualization tests using dyed water. The goal was to verify seal integrity for the device and to verify that no internal blockages had resulted in the fabrication processes. The water was perfused at mass flow rates over a range of 10-500 g/min using a programmable syringe pump. Tests were viewed under CCD video-microscopy and recorded to digital

video for archiving.

The initial testing with the propellant involved low-purity hydrogen peroxide at about 80% concentration; subsequent testing featured increasing concentrations up to the targeted value of 90%. Experiments were performed with the nozzle exit at ambient pressure, although future tests are planned in a vacuum chamber. The level of reaction noticeably increased with the concentration of hydrogen peroxide as expected from the chemical kinetics. Image sequences extracted from digital video recordings of test firings in the "zig-zag" and "diamond-pillar" designs are shown in Figures 5 and 6, respectively. The mass flow rate of propellant in each case was the targeted value of was in the range of 386-390 g/sec. As is clearly evident in these images, full decomposition of the propellant is not being achieved: multi-phase flow exists at the nozzle exit. In areas where the decomposition occurred, gas pockets and bubbles formed. In the earlier "zig-zag" design the gas tended to coalesce into larger bubbles which often pushed omni-directionally. In these designs, which did not feature the injector component, back-flow from the catalyst chamber into the reservoir was also observed. Similar behavior was also observed in the "diamond-pillar" design. As seen in Figure 6, portions of the catalyst chamber also became occupied with dispersed gas pockets. Looking carefully at the catalyst chambers in this image sequence, one sees this region become increasing blurred as the pillars become obscured by the gas formation. .In viewing live video, the pockets are much more apparent. They would intermittently become lodged between vertical pillars and would locally choke portions of the flow within the chamber. Given the close spacing the of pillars in this design (in comparison to the "zig-zag" design) it is quite possible that surface tension could have contributed to the sticking of the gas pockets. Because of the presence of the injector in this pillar design, back-flow into the reservoir was not observed. At the entrance to the catalysts chamber and primarily in the corners, there is an arc-ed darker region which under video appears to be an area of flow stagnation; this suggests that an inlet taper to the chamber width may be warranted in future designs. A final observation concerns the formation of gas prior to the

propellant entering the catalyst chamber (see Figure 6). This is due to the epoxy itself acting as a weak catalyst for the inlet propellant. While undesirable and worthy of correction, this is an artifact of the temporary laboratory plumbing connection which would not be present in an operational thruster.

In an attempt to quantify the level of decomposition occurring in the catalyst chamber, the liquid phase components of the exit flow for the "zig-zag" design (see Figure 5) were collected and analyzed for hydrogen peroxide concentration. The exit liquid consists of the unreacted propellant as well as some liquid phase water which had been produced in decomposition but had not evaporated; it was estimated that the latter constituted only about 3% of the volume. Hydrogen peroxide concentration was determined indirectly. The refractive index of the liquid was measured using a Brix refractometer and then correlated with published tables of the refractive index of aqueous hydrogen peroxide (Bureau of Aeronautics, 1955). The results are shown in Table 4. For this particular design, a linear extrapolation of these results suggest that complete decomposition would occur for a catalyst chamber length of 4.0 mm. While this length is still acceptable for a MEMS application, a more optimal design of the chamber would likely reduce this length. Similar measurements for the "diamond pillar" design have not yet been performed.

Finally, although not depicted here, some testing with nozzles of smaller divergence angles (15-20 degrees half-angle) has also been performed. Visual observations of the nozzle exit have indicated a somewhat erratic exit behavior in comparison with larger divergence angles nozzles. We hypothesize this is evidence of the viscous boundary layers filling much of the nozzle exit and further justifies the use of larger divergence angles in the design.

3.2 Current Technical Challenges and Tasks

While significant progress has been made towards the development of a prototype hydrogen peroxide microthruster, there are a number technical challenges to be overcome. The most critical challenge at

this time is that of achieving complete chemical decomposition of the propellant prior to the nozzle. Without complete decomposition, the thruster will not operate properly. It is clear that a detailed theoretical and computational investigation of this process is warranted in order to obtain engineering design models. The modeling of the decomposition process is a complex task requiring a fundamental knowledge of the coupled chemical kinetics and hydrodynamic behavior within the catalyst chamber. A particular challenging aspect of the modeling is due to the fact that the chemical reaction only occurs at the catalyst-coated surfaces; the "effect" of the reaction must therefore *propagate into* the bulk fluid . This is unlike most combustion processes which are volumetric phenomena and governed by field equations. The low Reynolds number in the micro-scale geometry creates additional hydrodynamic complications owing to the significance of viscous forces which extract energy from the flow. Taken together, the surface nature of the reaction and the MEMS geometry raise fundamental questions about the workings of the catalyzed decomposition process: Does the energy released at the surface generate flow "turbulence"[2] which mixes and brings the bulk liquid to the boundaries where it can undergo reaction? Alternatively, does the flow remain laminar and the heat generated at the boundary propagate into the bulk flow and vaporize the liquid propellant rather than decompose it? In this case, the efficiency of the thruster would be much lower since chemical energy remains stored in vaporized propellant. Moreover, the kinetic energy of the gaseous components will be different from those with complete decomposition which in turn will influence the inlet conditions for the supersonic nozzle. In support of the modeling, experiments are required which can precisely analyze the composition and proportions of the gas/liquids exiting from the nozzle. The use of mass spectroscopy has been considered; however, the similarity in the molecular weights of water and steam make it difficult to accurately distinguish the two. An alternative solution to this resolution problem which is currently

[2]The exact meaning of turbulence here is not necessarily in the traditional sense given the low Reynolds numbers of these flows.

being investigated is the use of an ultra-violet spectrometer.

Full numerical simulations of the nozzle flow are also required to better characterize and optimize thruster performance. While it is the consensus among published computational studies of micro-nozzle performance that viscous effects are significant, the quantified performance is also case specific. A computational model of our thruster nozzle operation with its multi-component gas flow will facilitate parametric studies leading to design optimization. This is especially significant for a MEMS-based thruster since the optimization can reduce the propellant mass requirements for the spacecraft. As with the decomposition modeling, supporting experimental measurements of thrust production are also needed to validate the numerical predictions. To ensure realistic exit conditions the experiments will be performed in a vacuum chamber at NASA/GSFC and thrust will be measured using a micro-Newton thrust stand.

3.3 Long-Term Challenges

Micro-Valves for Satellite Integration. For the ultimate incorporation of the MEMS thruster into nanosats there are microfluidic challenges. Specifically there is the issue of implementing a micro-valve which allows the propellant flow to be regulated (either continuously or in a digital manner). To this end, NASA/GSFC is initiating a study with an industrial partner to exam potential micro-valve concepts for this MEMS thruster. Valving is a non-trivial problem to achieve in a MEMS/nanosat configuration. The micro-valve mechanism must be both small in scale and self-contained for nanosat purposes, yet it most also be able to provide reliable seals at pressures on the order of 5 psi or more. Most current MEMS-based micro-valve concepts that have been reported in the literature rely upon actuation by some externally applied electrostatic, electromagnetic, or pneumatic force (see, for example, Ho and Tai, 1998); as such, integration into a nanosat configuration may be problematic. Micro-valve issues in the context of small spacecraft propulsion is further discussed in Mueller et al.

(2000).

Propellant Storage. Another major challenge that must be addressed for the deployment of the hydrogen peroxide microthruster is that of stable, long-term propellant storage. Even in the absence of a catalyst, hydrogen peroxide is known to undergo auto-decomposition; a consequence of this is the corresponding rise in reservoir pressure. The increase in pressure could, in turn, have implications for leakage in a MEMS-based system unless a venting mechanism is included; the additional of chemical stabilizers are unacceptable since they dramatically degrade the performance in the catalyst chamber of the thruster. The incorporation of a venting mechanism in the storage system introduces additional and significant engineering challenges and is therefore undesirable from design perspective. Fortunately, the rate of auto-decomposition is relatively slow and decreases with temperature. At room temperature, auto-decomposition occurs at a rate of approximately 1% a year at and this rate doubles for each increase of 15 degrees Fahrenheit (Chemical Propulsion Information Agency, 1984). Hydrogen peroxide storage as low as 12 degrees Fahrenheit is permissible, so the space environment can be used to greatly slow the auto-decomposition rate provided the possibility of solar heating is accounted for. The combination of a reduced auto-decomposition rate at low temperatures and the limited mission durations planned for nanosatellites (< 1 year typically), it may be possible to design a propellant storage system which does not require venting. A related issue concerns the material compatibility of the storage tank. Virtually all materials serve as some form of catalyst for the decomposition of the hydrogen peroxide and so even a weak catalyst could pose tank pressurization problems over an extended mission duration. The identification of appropriate storage tank design - including the possibility of an internal liner between the tank wall and the hydrogen peroxide - is thus an important challenge which must be overcome.

3.4 Alternative Monopropellants

The choice of hydrogen peroxide as a monopropellant in this work has been largely motivated by its non-toxicity and relative ease of handling; this is attractive for purposes of prototype development. Clearly there are limitations to its use in actual spacecraft application. The primary difficulty that has been identified is that of long term storage. Other chemical propellants - most notably hydrazine - are known to be quite stable over long periods of time (>15 years). Further, hydrazine offers a higher performance as a propellant. The main difficulty is its high toxicity level. The eventual goal is to extend the MEMS-based catalytic propulsion mechanism developed for the hydrogen peroxide to a higher performance microthruster based upon the hydrazine.

4 Conclusions

Future generations of small spacecraft planned by NASA and other agencies call for unique and dramatically reduced micropropulsion concepts. Aside from simply satisfying thrust levels on the order of micro- and milli- Newtons, the propulsion systems themselves must be satisfy stringent size and power constraints. Microelectromechanical systems represents an enabling technology through which the micro-thruster design challenge can be met. In this article we have described progress towards the development of a monopropellant microthruster prototype which relies upon the catalyzed chemical decomposition of high concentration hydrogen peroxide for the propulsion mechanism. Though several engineering challenges remain, the results thus far are encouraging. The primary difficulty encountered has been that of achieving complete chemical decomposition of the propellant within the MEMS geometry. As complete decomposition has been achieved in macro-scale thrusters for decades, there are evidently aspects of the (coupled) chemical kinetics and hydrodynamics that are particular to the micro-scale; investigations dedicated to obtain a fundamental understanding of this behavior are both warranted and planned in the future. Once the decomposition problem has been solved, it is our belief

that this design concept will be capable of providing the targeted level of thrust and will serve as the cornerstone of the complete micropropulsion system.

Acknowledgments

The authors are very grateful to a number of individuals who have contributed to the MEMS catalytic thruster program at NASA - Goddard Space Flight Center and, either directly or indirectly, to the material presented in this article. The authors would also like to acknowledge Dennis Asato, Jon Lewis, Bob Estes and Chris Anders of the NASA/Goddard Propulsion Branch for their ongoing work on this project and for providing some of the graphical and photographic materials used in this article. Brent Mott and Tina Chen of the NASA/Goddard Detector Branch are to be commended for their expertise in the reactive ion etching of the microthruster geometries used in this work. The work at NASA/GSFC was supported under NASA's Cross Enterprise Technology Program; additional support for an in-residence research leave (DLH) was provided by the NASA/ASEE Faculty Research Fellowship Program.

References

A. A. Alexeenko, S.F. Gimelshein, D.A. Levin, and R.J. Collins, 2000, "Numerical modeling of axisymmetric and three-dimensional flows in MEMS nozzles," Proceedings of the 36th AIAA/ASME/SAE/ASEE Joint Propulsion Conference and Exhibit, Huntsville, AL.

Ė. Antonsson and S.W. Janson, "MEMS Microthruster Digital Propulsion System," Proceedings of the Joint AFRL/MIT Formation Flying and Micro Propulsion Workshop, October 1998.

R.L. Bayt, A.A. Ayon, and K.S. Breuer, 1997, "A Performance Evaluation of MEMS-based Micronozzles," AIAA 97-3169, Proceedings of the 33rd AIAA/ASME/SAE/ASEE Joint Propulsion

Conference and Exhibit, Seattle WA.

R.L. Bayt and K.S. Breuer, 1998, "Viscous effects in supersonic MEMS-fabricated micronozzles," Proceedings of the 3rd ASME Microfluids Symposium, Anaheim CA.

R.L. Bayt, and K.S. Breuer, 2001, "System design and performance of hot and cold supersonnic microjets," AIAA Paper 2001-0721.

M. Bettner and R. Humble, "Polyethylene and Hydrogen Peroxide Hybrid Testing at the United States Air Force Academy," Proceedings of the 1st Annual Hydrogen Peroxide Conference, Surrey U.K. 1998.

J. Blandino and R. Cassady, 1998, "Propulsion requirements and options for the New Millennium Interferometer (DS-3) Mission," AIAA Paper 98-3331, Proceedings of the 34th AIAA/ASME/SAE/ASEE Joint Propulsion Conference & Exhibit, Cleveland, OH.

Bureau of Aeronautics, 1955, *Handbook - Field Handling of Concentrated Hydrogen Peroxide, NAVAER 06-25-501.*

Chemical Propulsion Information Agency, 1984, "Hazards of Chemical Rockets and Propellants," Publication 394, Volume III.

A.R. Choudhurri, B, Baird, S.R. Gollahalli, and S.J. Schneider, 2001, "Effects of geometry and ambient pressure on micronozzle flow," AIAA 2001-3331, Proceedings of the 37th AIAA/ASME/SAE/ASEE Joint Propulsion Conference & Exhibit, Salt Lake City, UT.

A.D. Gallimore, 2001, "Review of the EP activities of US academia," AIAA 2001-3227, 37th AIAA/ASME/SAE/ASEE Joint Propulsion Conference & Exhibit, Salt Lake City, UT.

W. J. Hesse and N.V.S. Mumford, Jr., 1964, *Jet Propulsion for Aerospace Applications 2nd ed.*, Pitman Publishing Co., New York.

S.W. Janson, 1994, "Chemical and electric micropropulsion concepts for nanosatellites", AIAA-94-2998, 30th AIAA/ASME/SAE/ASEE Joint Propulsion Conference & Exhibit, Indianapolis, IN.

W. Janson and Henry Helvajian, 1999, "MEMS, Microengineering, and Aerospace Systems," AIAA Paper 99-3802.

S. Janson, H. Helvajian, W. Hansen, and J. Lodmell, 1999, "Batch-Fabricated CW Microthrusters for Kilogram-Class Spacecraft," AIAA 99-2722, Proceedings of the 35th AIAA/ASME/SAE/ASEE Joint Propulsion Conference & Exhibit, Los Angeles, CA.

A. Ketsdever and J. Mueller, 1999, "Systems considerations and design options for microspacecraft propulsion systems," AIAA Paper 99-2723, Proceedings of the 35th AIAA/ASME/SAE/ASEE Joint Propulsion Conference & Exhibit, Los Angeles, CA.

D. Lewis, S. Janson, and R. Cohen, 2000, "Digital Micro-Propulsion Project," Sensors and Actuators A 2000. pp. 143-154

R. Moser, D. Collins, A. Das, R. Ferber, G. Jaivin, R. Madison, J. Smith, and M. Stallard, 1999, "Novel missions for next generation microsatellites: the results of a joint AFRL-JPL study," Proceedings of the 13th AIAA/USU Conference on Small Satellites, Logan, UT.

J. Mueller, 1997, "Thruster options for microspacecraft: a Review and evaluation of existing hardware and emerging technologies, AIAA Paper 97-3058.

J. Mueller, S. Vargo, D. Barne, I. Chakraborty, and W. Tang, 2000, "Micro-isolation valve concept: initial results of a feasibility study," in *Micropropulsion for Small Spacecraft - Progress in Astronautics and Aeronautics*, M. Micci and A. Ketsdever, eds., vol. 187, AIAA, Reston, Va., p. 399-422.

J. Mueller, 2000, "Thruster options for microspacecraft: a Review and evaluation of the state-of-the art and emerging technologies, in *Micropropulsion for Small Spacecraft - Progress in Astronautics and*

Aeronautics, M. Micci and A. Ketsdever, eds., vol. 187, AIAA, Reston, Va., p. 45-137.

P.V. Panetta, 1998, "NASA-GSFC Nano-Satellite Technology Development," Proceeding of the 12th AIAA/USU Conference on Small Satellites, Logan, UT.

J. Pollard, C. Chao, and S. Janson, "Populating and Maintaining Cluster Constellations in Low-Earth Orbit," AIAA 99-2871, Proceedings of the 35th AIAA/ASME/SAE/ASEE Joint Propulsion Conference & Exhibit, Los Angeles, CA, June 1999.

B. Reed, 1998, "Micropropulsion Activities at NASA Lewis Research Center," Proceedings of the Joint AFRL/MIT Formation Flying and Micro Propulsion Workshop, October 1998.

Reichach J.G., Sedwick R.J., and Martinez-Sanchez, M. , 2001, "Micropropulsion system selection for precision formation flying satellites," AIAA 2001-3646, 37th AIAA/ASME/SAE/ASEE Joint Propulsion Conference & Exhibit, Salt Lake City, UT.

M.A. Saad, 1993, *Compressible Fluid Flow 2nd ed.*, Prentice-Hall, Inc., New York.

J.J. Sellers, R. Brown, and M. Paul, "Practical Experience with Hydrogen Peroxide Catalysts," Proceedings of the 1st Annual Hydrogen Peroxide Conference, Surrey, UK, 1998.

G. Spanjers, 1998, "Micro-Propulsion Research at Air Force Research Laboratory," Proceedings of the Joint AFRL/MIT Formation Flying and Micro Propulsion Workshop.

Thomas, M.K., Zakrzwski, C. and Hitt, D.L., 2000, "Progress Towards a Hydrogen Peroxide Catalytic MEMS Micro-Thruster", Annual Meeting of the American Physical Society's Division of Fluid Dynamics, Washington, DC.

D. Weidow and J. Bristow, "NASA/DOD Nano-Satellites for Distributed Spacecraft Control," Proceeding of the 13th AIAA/USU Conference on Small Satellites, Logan, UT August 1999.

D. Zelesnik, M.M. Micci, and L. N. Long, 1994, "Direct simulation Monte Carlo model of low Reynolds number nozzle flows," J. of Propulsion and Power, vol. 10, p. 546-55.

List of Tables

Table 1- Typical nanosat operating requirements. The quantities "impulse bit" and "specific impulse" are important in satellite propulsion dynamics. The impulse bit is simply the time integral of the thrust over the duration of the burn, whereas the specific impulse is the thrust normalized by the mass flow rate of the propellant.

Table 2 - A survey of some micropropulsion initiatives in academia, government and industry in recent years. This listing is meant to be representative of current efforts in this area and to provide the reader with an appreciation of the activity; it is not intended as an exhaustive review.

Table 3 - A summary of the design and operating parameters for the supersonic micro-nozzles based upon quasi-1D isentropic flow theory.

Table 4 - Measured decomposition efficiencies of hydrogen peroxide propellant in the "zig-zag" design as a function of catalyst chamber length. The efficiency is defined as the percentage of complete decomposition that has occurred as evidenced by the concentration of the hydrogen peroxide in the exit liquid. Concentration is determined indirectly measuring the refractive index of the liquid using a Brix refractometer and correlating with tabulated values for hydrogen peroxide; the estimated accuracy of the measurement is ±1%. The mass flow rate was approximately 400 g/sec and the inlet concentration of the hydrogen peroxide propellant was 90% .

List of Figures

Figure 1 - A schematic drawing of the propulsion mechanism for the HTP micro-thruster. High purity hydrogen peroxide is delivered from a plenum an approximate pressure of 5-6 psia to a silver-based catalytic chamber. In the catalytic chamber the HTP undergoes a highly exothermic chemical decomposition which expands the liquid propellant into gaseous products which are in turn fed to the inlet of a converging/diverging nozzle. In the nozzle the gas flow becomes supersonic at the throat and continues to accelerate, producing a thrust upon its exit.

Figure 2 - Mechanical drawings showing top views of two microthruster design geometries that have been developed. All dimensions are in microns. In the actual thruster this geometry is etched to a depth of 100-300 in the substrate. The basic thruster consists of an inlet with filters, a catalyst chamber, and a converging/diverging nozzle. (a) The original "zig-zag" design with a catalyst chamber consisting of vertical walls which extend from the base of the substrate to the top of the thruster. There is no injector incorporated in this design. (b) The more recent "diamond pillar" catalytic design. For the configuration shown, the pillars have square cross sections with 40 sides and are rotated 45 degrees with respect to the catalyst chamber flow axis. The perpendicular distance between adjacent pillars is 20 . Note the addition of the injector in this design.

Figure 3 - A sequence of SEM photos showing the microfabrication results for the "diamond pillar" thruster. (top) The full thruster, composed of an inlet plenum, an injector, a catalyst chamber and a supersonic nozzle. (middle) A close-up of the catalyst chamber with the diamond-pillar configuration. To evaluate the uniformity of the vertical etching, some of the pillars have been intentionally

destroyed to reveal features near the bottom. (bottom) Close-up of the toppled pillars. For this thruster design, the catalyst chamber is 2178 long, 1103 wide and 100 deep; the nozzle throat is 90 .

Figure 4 - Digital photograph of the completed MEMS "diamond pillar" micro-thruster. A top view is shown, with the inlet at the bottom and the nozzle at the top of the figure. To provide a reference length scale, a US penny is included in the background.

Figure 5 - Digital photographs of a test firing of a "zig-zag" thruster. This particular configuration is similar to that shown in Figure 2(a) except that the catalyst chamber is divided into piece-wise linear microchannel sections. This piece-wise configuration was intended to increase the length of the catalyst chamber (2.5 mm here) while still occupying the same area on the substrate; the motivation was to lengthen the chamber to promote a higher degree of decomposition. From top to bottom: The thruster under static conditions; propellant begins filling the chamber; under quasi-steady conditions, the multi-phase flow exiting the nozzle is primarily in the gaseous state indicating a high degree of decomposition and/or vaporization in the thruster. The mass flow rate was ~395 g/sec.

Figure 6 - Frames extracted from a digital video recording of a test firing of a "diamond pillar" thruster with a mass flow rate of ~386 g/sec. In this configuration the catalyst chamber length is 1088 , or 50% that of the design shown in Figure 2b. (Top) The thruster at the start of the firing. (Middle) The thruster after an elapsed time of 1.7 sec after firing; a multi-phase flow high in gas content. (Bottom) The thruster after an elapsed time of 13.1 sec. As the flow becomes quasi-steady the multi-phase exit flow is quite energetic and high in gas content suggesting a significant degree of decomposition and/or vaporization has occurred. The energy of the exit flow is much more apparent

under real-time video. A qualitative assessment is that the exit flow in this design is more energetic than in the "zig-zag" design.

Propulsion System Parameter	Target Value or Range
Thrust Level	**1-1000 N**
Impulse Bit	**1-100 N-sec**
Specific Impulse	**160 sec**
Mass	**< 0.1 kg**
Power Consumption	**< 1 W**
Volume	**< 1 cm^3**
Operating Temperature	**< 1700 K**

Table 1

Nozzle Parameter	Design Value
Thrust Level	500 N
Maximum Specific Impulse	180 sec
Specific Impulse Efficiency	80%
Mass Flow Rate	400 g/sec
Throat Area	9000 ^{2}
Inlet Pressure	5-6 psia
Outlet Pressure	~ 0 psia
Inlet Mach Number	0.05
Exit Mach Number	3.3
Reynolds Number (throat)	450

Table 3

Catalyst Chamber Length	Percentage of Decomposition
1.0 mm	70%
1.5 mm	75%
2.5 mm	85%

Table 4

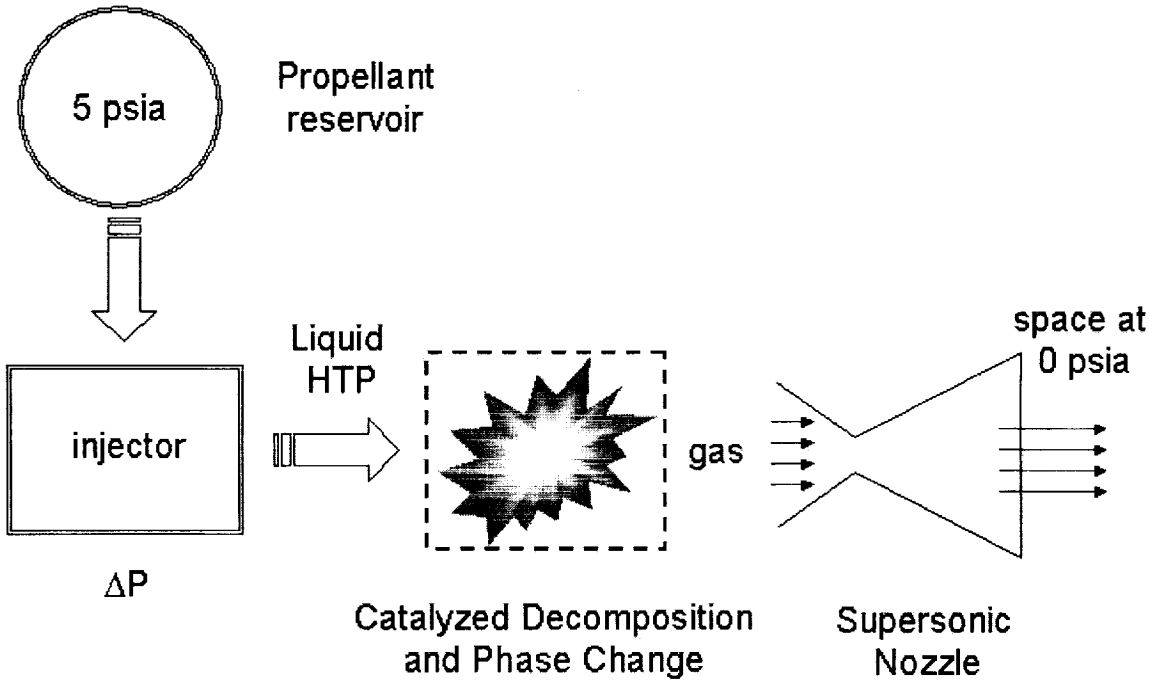
5 psia
Propellant reservoir
injector
ΔP
Liquid HTP
gas
space at 0 psia
Catalyzed Decomposition and Phase Change
Supersonic Nozzle

Figure 1

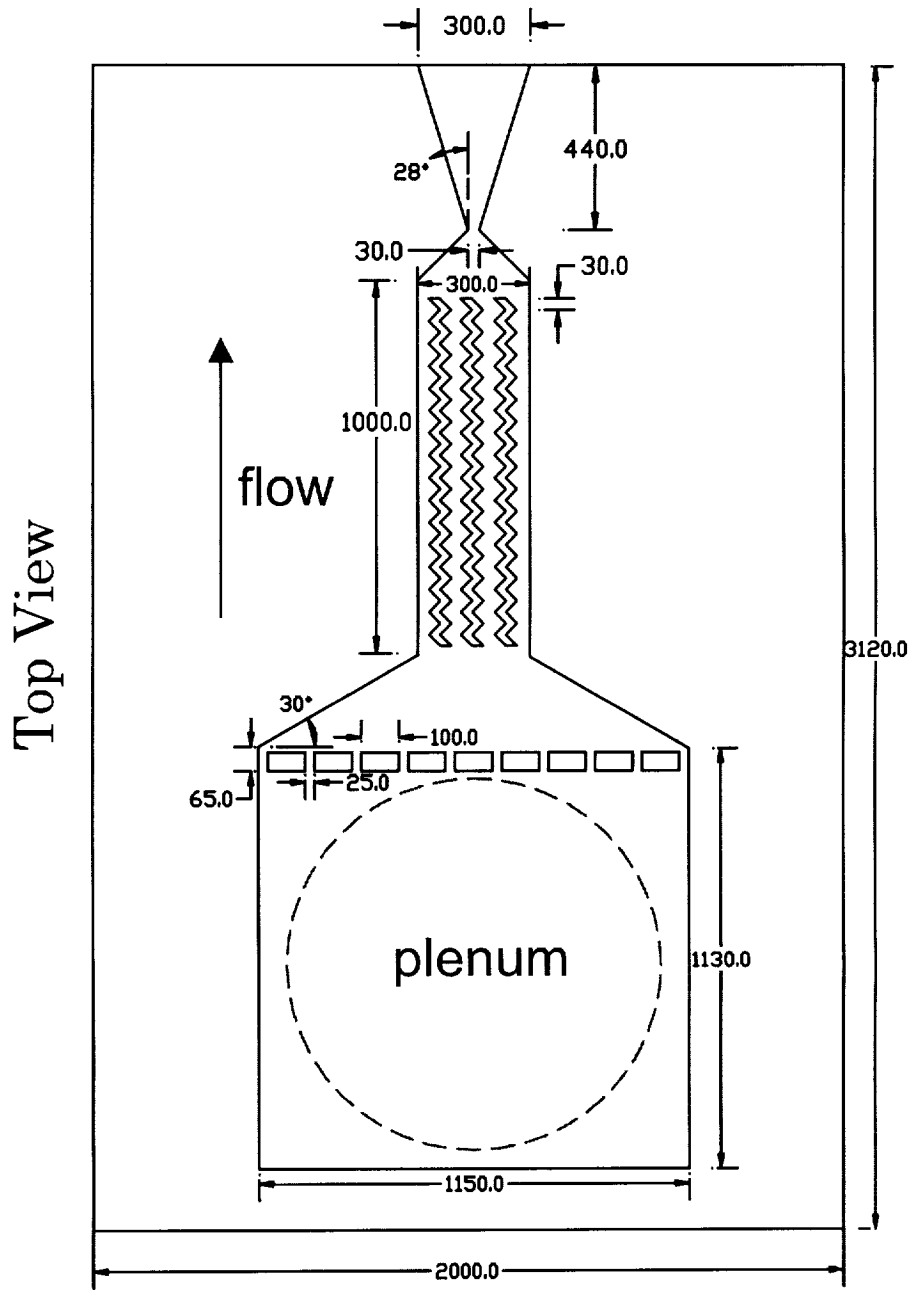
300.0
440.0
28°
30.0
30.0
300.0
1000.0
flow
Top View
3120.0
30°
100.0
65.0
25.0
plenum
1130.0
1150.0
2000.0

Figure 2(a)

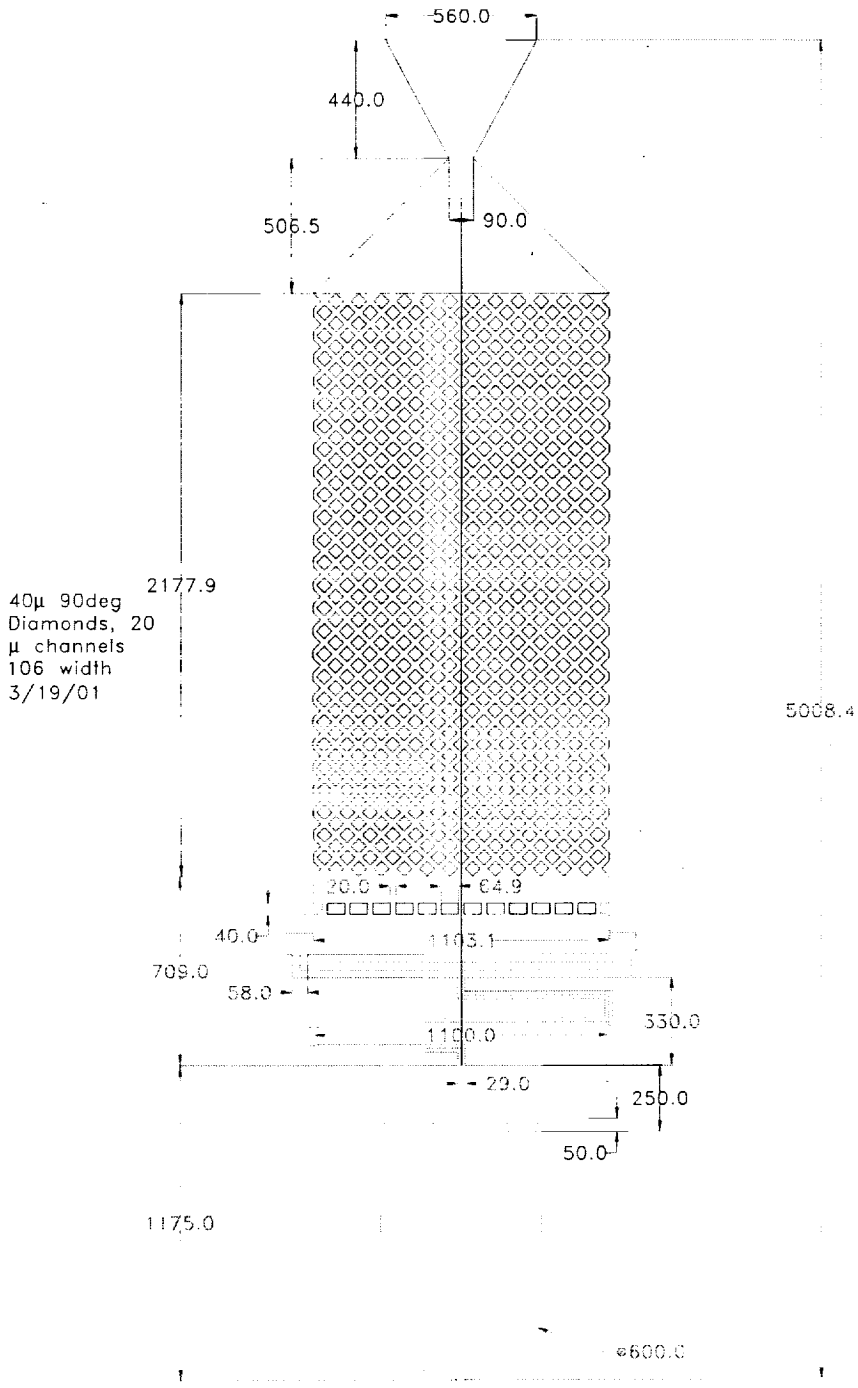
560.0
440.0
506.5
90.0
2177.9
40μ 90deg
Diamonds, 20
μ channels
106 width
3/19/01
5008.4
20.0
64.9
40.0
1103.1
709.0
58.0
330.0
1100.0
29.0
250.0
50.0
1175.0
ø600.0

Figure 2(b)

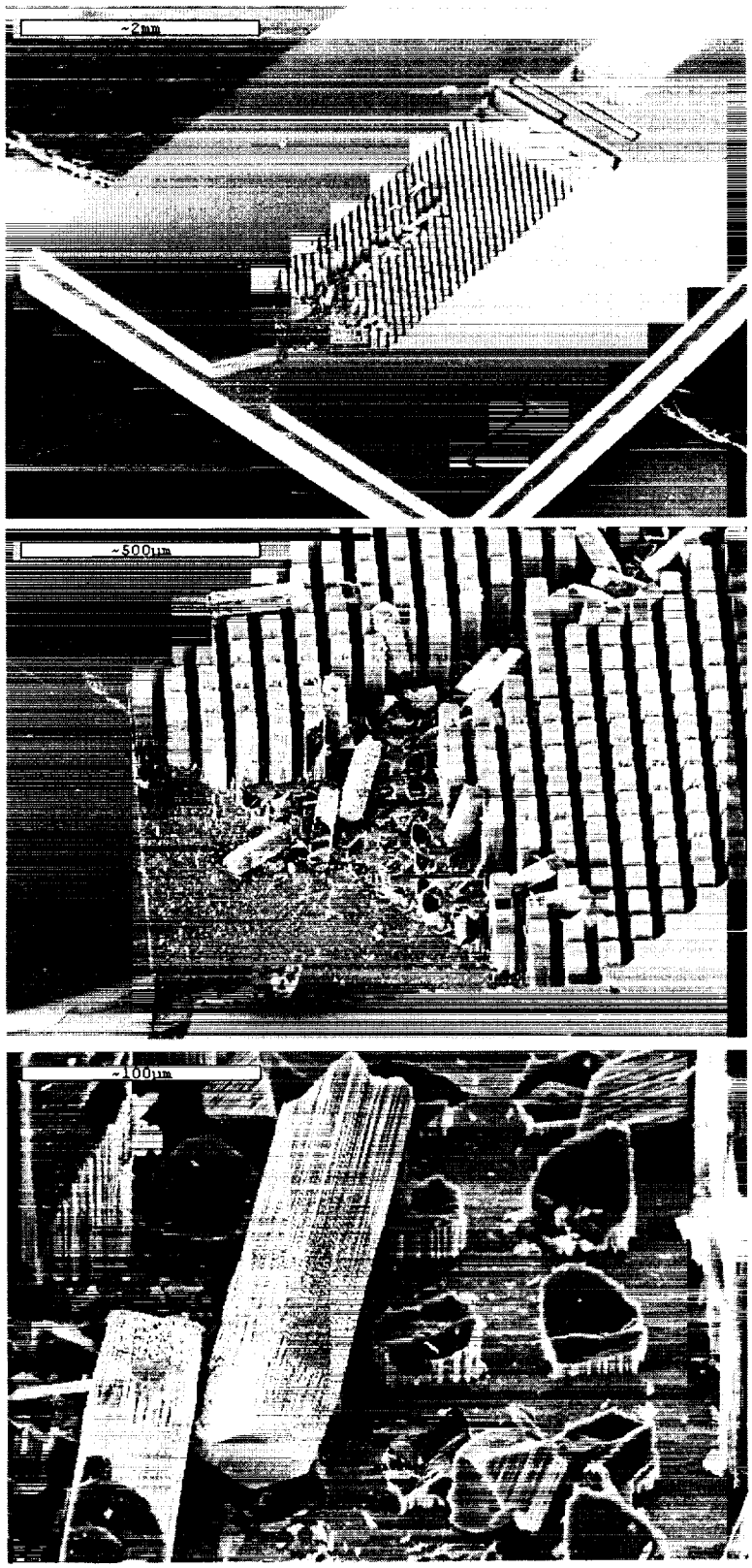

Figure 3

Figure 4

Figure 5

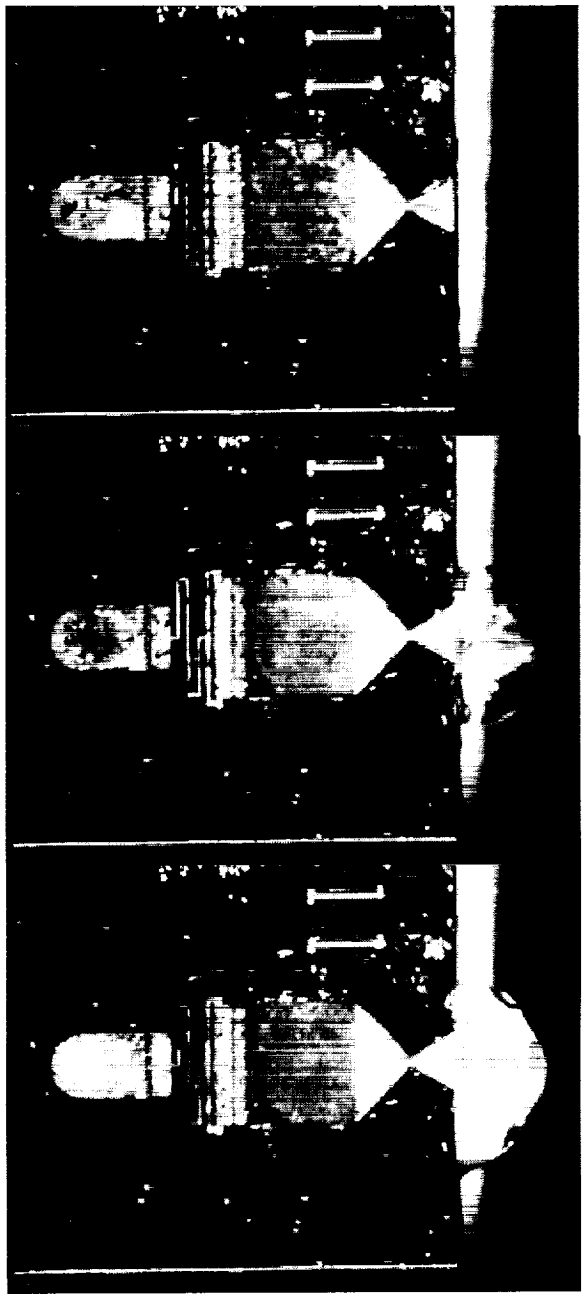

Figure 6